Vibration band gaps in double-vibrator pillared phononic crystal plate

Hao-Jiang Zhao, Hong-Wei Guo, Ming-Xing Gao, Rong-Qiang Liu', and Zong-Quan Deng

Citation: Journal of Applied Physics 119, 014903 (2016); doi: 10.1063/1.4939484

View online: http://dx.doi.org/10.1063/1.4939484

View Table of Contents: http://aip.scitation.org/toc/jap/119/1

Published by the American Institute of Physics

Articles you may be interested in

Flexural vibration band gaps in a double-side phononic crystal plate Journal of Applied Physics **118**, 044906 (2015); 10.1063/1.4927627

Ultrathin lightweight plate-type acoustic metamaterials with positive lumped coupling resonant Journal of Applied Physics **121**, 015102 (2017); 10.1063/1.4972839

Local resonator with high-static-low-dynamic stiffness for lowering band gaps of flexural wave in beams Journal of Applied Physics **121**, 044902 (2017); 10.1063/1.4974299

Low-frequency band gap and defect state characteristics in a multi-stub phononic crystal plate with slit structure Journal of Applied Physics **121**, 015106 (2017); 10.1063/1.4973577

Dual-directionally tunable metamaterial for low-frequency vibration isolation Applied Physics Letters **110**, 021907 (2017); 10.1063/1.4974034

Ultra-wide acoustic band gaps in pillar-based phononic crystal strips Journal of Applied Physics **118**, 214902 (2015); 10.1063/1.4936836





Vibration band gaps in double-vibrator pillared phononic crystal plate

Hao-Jiang Zhao,^{1,2} Hong-Wei Guo,¹ Ming-Xing Gao,¹ Rong-Qiang Liu,^{1,a)} and Zong-Quan Deng¹

¹School of Mechatronics Engineering, Harbin Institute of Technology, Harbin 150001, People's Republic of China

²Changchun Institute of Optics, Fine Mechanics and Physics, Chinese Academy of Sciences, Changchun 130033, People's Republic of China

(Received 5 September 2015; accepted 21 December 2015; published online 5 January 2016)

This paper proposes a double-vibrator three-component pillared phononic crystal plate and theoretically studies the properties of vibration band gaps of this plate. The band structures and the displacement fields of the eigenmodes are calculated by the finite element method. Comparing the transmission power spectrums of the vibrations in the plate, the flexural vibration gap is proved more useful than the longitudinal vibration gap. The influence of the lattice constant, the height, and diameter of the pillars on the flexural vibration gaps are investigated. A supercell composed of the uni-vibrator and the double-vibrator unit cells is also investigated, and the analysis shows that the starting frequencies of the gaps in this supercell structure depend on the features of its pillars. This research can be used in the low frequency vibration insulation of plate structures. © 2016 AIP Publishing LLC. [http://dx.doi.org/10.1063/1.4939484]

I. INTRODUCTION

The propagation of elastic waves and vibrations in phononic crystals (PCs) has been extensively studied for the past two decades. 1-19 With appropriate geometric and material parameters, PCs can obtain acoustic band gaps (ABGs), where vibrations are prohibited. The existence of ABGs makes PCs potential in the area of vibration insulation. Bragg scattering^{1,2} and local resonance (LR)^{3,4} are the two main mechanisms for the creation of ABGs. The elastic wave length corresponding to the frequency range of the ABGs obtained by the Bragg scattering PC has the same order of magnitude with the lattice constant. Therefore, to get low frequency ABGs, the lattice constant of the Bragg scattering PC should be large enough, which goes against noise reduction and vibration insulation when the geometric size is limited. Fortunately, LR PCs can obtain low frequency ABGs with a much smaller lattice constant.

Recently, the vibration characteristics of the pillared PC plates possessing LR gaps have received increasing attention. 4-19 There are pillared PC plates composed by one, 5-9 two, ^{10–18} or three kinds of materials. ^{11,13,19} Pennec *et al.* ¹⁰ investigated theoretically a two-component pillared PC plate and found that the opening of its gap requires appropriate geometrical parameters, in particular, the thickness of the homogeneous plate and the height of the dots. Oudich et al. 11 investigated the influence of geometric parameters on the band gaps of two-component and three-component pillared PC plates and pointed out that the low-frequency band gaps is opened by the coupling of the Lamb mode and pillar mode. Yu et al. 15 found that ultra-low frequency band gaps can be obtained in PC plate composed of a rubber base plate with uniformly distributed steel pillars, but a thin rubber base plate is too flexible to be a strutting piece.

The other important influence factor of ABGs in pillared PC plates is their geometric parameters. Hsu⁶ proposed the pillars with a "neck" in the PC slab with stepped resonators and proved that the pillars exhibit both local resonance band gaps and Bragg band gaps. Bilal and Hussein⁸ found that trampoline effect caused by periodic holes in the base plate of pillared PC plates can enlarge the ABGs by up to a factor of 4. Tapered pillars were theoretically proved more effectively in opening lower ABGs than cylindrical pillars. ¹⁴ The LR PCs are usually simplified as spring-mass models. ⁴ Xiao et al. studied the vibration properties of PC plate composed of periodic spring-mass vibrators on the side of a thin homogeneous plate and found that the resonance frequencies of the spring-mass vibrators greatly affect the band gaps.

If one complex pillar (containing two kinds of material) is treated as a local resonance vibrator, then besides the above uni-vibrator in the unit cell, Xiao *et al.*¹⁶ also proposed LR PC plates consisting of a periodic array of double-stacked beam-like resonators attached to a thin homogeneous plate, which means two vibrators in one unit cell. In this study, we propose a double-vibrator (rubber-steel-rubber-steel layers) three-component pillared PC plate (DVTCPPCP) on the basis of the traditional uni-vibrator (rubber-steel layers) three-component pillared PC plate (UVTCPPCP) and study the propagation characteristics of flexural vibration and longitudinal vibration in the plate by numerical method.

II. MODEL AND METHOD

Fig. 1 shows the proposed DVTCPPCP and its unit cell. The double-vibrator pillar in the unit cell is composed of four layers of cylindrical slices (rubber stub-steel cap-rubber stub-steel cap) with the same diameter *d*. Treating one rubber stub and one steel cap as one vibrator, then each pillar in this structure has two vibrators. The *z*-axis is perpendicular to the plate. The lattice constant, the thickness of base plate, and

a) Author to whom correspondence should be addressed. Electronic mail: liurqhit@163.com.

FIG. 1. (a) DVTCPPCP arranged in a square lattice, (b) its unit cell, (c) the first Brillouin zone, and (d) meshing of the unit cell.

the height of cylindrical layers are denoted by a, e, and h_i (i = 1-4). The materials' parameters used in the calculation are shown in Table I, and all materials are assumed to be elastically isotropic.

The vibration band structures of the proposed pillared PC plates are calculated using the finite element method (FEM). COMSOL Multiphysics, a commercial software, is adopted to implement the FEM calculation procedures. Given the periodicity of the structure, only one unit cell is needed in the calculation. The unit cell used to calculate the band structures in COMSOL Multiphysics is shown in Fig. 1(d). Stress-free boundary conditions are used for the free surfaces, and periodic boundary conditions according to the Bloch-Floquet theorem¹¹ are used for the interfaces between the nearest unit cells

$$u_j(x+a,y+a) = u_j(x,y)e^{i(k_x a + k_y a)}, \quad (j = x, y, z),$$
 (1)

where u_j denotes the elastic displacement vector; (x, y, and z) are the position vectors; and k_x and k_y are Bloch wave vectors limited in the irreducible first Brillouin zone (1BZ), as shown in Fig. 1(c). The band structures and the eigenmodes can be obtained by calculating the eigenvalues and eigenvectors of the wavevectors.

III. NUMERICAL RESULTS AND ANALYSES

A. Band structures and eigenmodes

In this section, the band structure of the DVTCPPCP is calculated using the FEM, as shown in Fig. 2. The calculation examples take the following structure parameters: $a=50\,\mathrm{mm},\ e=5\,\mathrm{mm},\ d=45\,\mathrm{mm},\ \mathrm{and}\ h_\mathrm{i}=5\,\mathrm{mm}\ (i=1-4).$ To verify the existence of the vibration band gaps, the transmission power spectrums of flexural vibration (Fig. 2(a)) and longitudinal vibration (Fig. 2(d)) in the limited periodic (6×6) PC plate with free boundary condition are calculated by using the FEM. To get the transmission power spectrums, a displacement excitation d_in is imposed on one end of the plates, and on the other end of the plate the average

TABLE I. Material parameters used in calculations.

Material	Young's modulus (10^6N/m^2)	Mass density (kg/m³)	Poisson's ratio
Rubber	0.12	1300	0.47
Aluminum	72 100	2800	0.35
Steel	210 000	7800	0.29

displacement response d_{out} is picked up. The transmission spectra L_{d} is defined as

$$L_{\rm d} = 20 \log \frac{|d_{\rm out}|}{|d_{\rm in}|}.$$
 (2)

These band structures of dispersion relations include the propagation of multiple vibrations. To pick out the starting frequency f_s (from which frequency the gap starts) and the cutoff frequency f_c (at which frequency the gap ends) of the flexural vibration band gaps (FVBGs) and the longitudinal vibration band gaps (LVBGs), the relative modes must be distinguished from the other modes. The displacement fields of the eigenmodes labeled in Figs. 2(b) and 2(c) are shown in Fig. 3.

For modes B₁-B₄, the dominant vibration along the z-axis couples with the antisymmetric Lamb mode of the base plate, so the modes are involved in the formation of the FVBGs. Modes B₁ and B₂ correspond with the starting and cutoff frequencies of the first FVBG, respectively. In mode B₁, the vibration energy concentrates on the two steel caps in the double-vibrator pillar which vibrates along the same direction. In mode B2, the dynamic balance is obtained by the inverse vibration of the base plate and the lateral steel cap (h_1) along the z-axis, with the middle steel layer (h_3) as the stationary layer. Meanwhile, flexural vibration shows significant attenuation in the frequency range of the first FVBG in Fig. 2(a), which indicates that the first FVBG exists in this frequency range (from 145 Hz to 266 Hz). Modes B₃ and B₄ correspond with the starting and cutoff frequencies of the second FVBG, respectively. Mode B₃ concentrates the vibration energy in the pillars with the inverse vibration of the two steel caps and keeps the base plate stationary. In mode B_4 , the lateral steel cap (h_1) acts as the stationary layer, while the inverse vibration of the base plate and middle steel layer (h_3) achieve dynamic balance. Similarly, flexural vibration shows significant attenuation in the frequency range between modes B₃ and B₄ in Fig. 2(a), which indicates that second FVBG exists at this frequency range (from 365 Hz to 411 Hz).

For modes B_5 - B_8 , the dominant vibration in the xy plane couples with the symmetric Lamb mode of the base plate, so the modes are involved in the formation of the LVBGs. Modes B_5 and B_6 correspond with the starting and cutoff frequencies of the first LVBG. Mode B_5 concentrates vibration energy on the whole body movement of the double-vibrator pillar along the xy plane. While Mode B_6 takes the middle

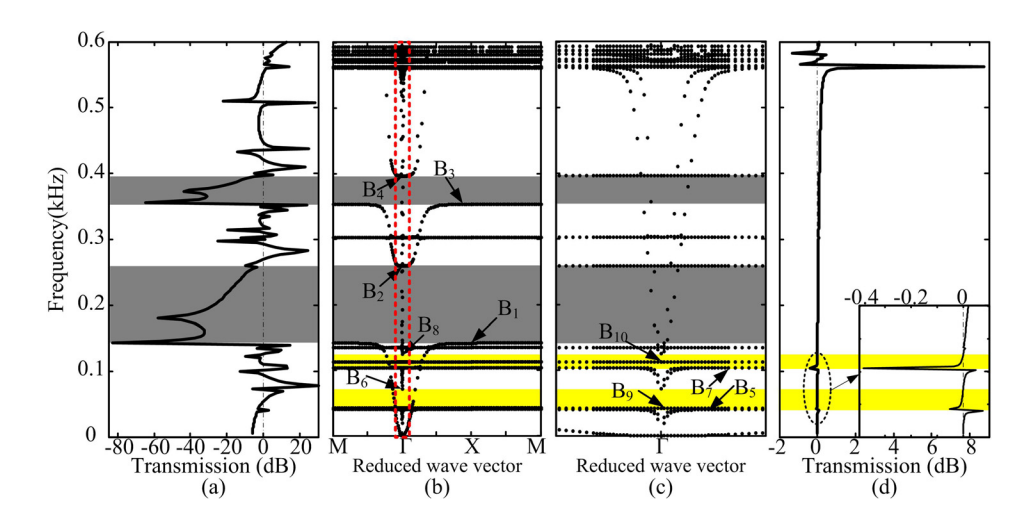


FIG. 2. Band structure and the transmission power spectrums of the DVTCPPCP: (a) transmission power spectrum of flexural vibration; (b) band structure; (c) a zoom near Γ point; (d) transmission power spectrum of longitudinal vibration.

layer as the stationary layer and achieves dynamic balance of the inverse vibration of the lateral steel cap (h_1) and the base plate in the xy plane. Meanwhile, longitudinal vibration shows attenuation in the corresponding frequency range in Fig. 2(d), which indicates that the first LVBG exists in this frequency range (from $40\,\text{Hz}$ to $72\,\text{Hz}$). Modes B_7 and B_8 correspond with the starting and cutoff frequencies of the second LVBG. In mode B₇, the base plate remains still, and the horizontal displacement of middle steel layer (h_3) twists the lateral steel cap (h_1) . In mode B_8 , the middle steel layer (h_3) and the base plate move along the reverse horizontal direction; meanwhile, the horizontal displacement of the middle steel layer (h_3) twists the lateral steel cap (h_1) . Similarly, longitudinal vibration shows attenuation at the corresponding frequency range in Fig. 2(d), which indicates that the second LVBG exists in this frequency range (from 104 Hz to 125 Hz).

For modes B_9 and B_{10} , the vibration energy is mainly concentrated at the rotating pillars, which means that no coupling with the longitudinal or flexural vibration in the base plate occurs. What makes modes B_9 and B_{10} different is that each pillar in mode B_9 has the same rotation direction, whereas the lateral steel caps and middle steel caps in mode B_{10} rotate in opposite directions.

Comparing the transmission power spectrum of the flexural vibration (Fig. 2(a)) with that of the longitudinal vibration (Fig. 2(d)), one can find that the attenuation in the FVBGs is much more obvious than that in the LVBGs. Hence, the following research in this paper is mainly on the FVBGs of the DVTCPPCP. Fig. 4 shows local views of the corresponding vibration modes of the starting and cutoff frequencies of the first two FVBGs in the DVTCPPCP with $6a \times 6a$ unit cells. Vibration modes of these unit cells, respectively, correspond with the eigenmodes B_1 , B_2 , B_4 ,

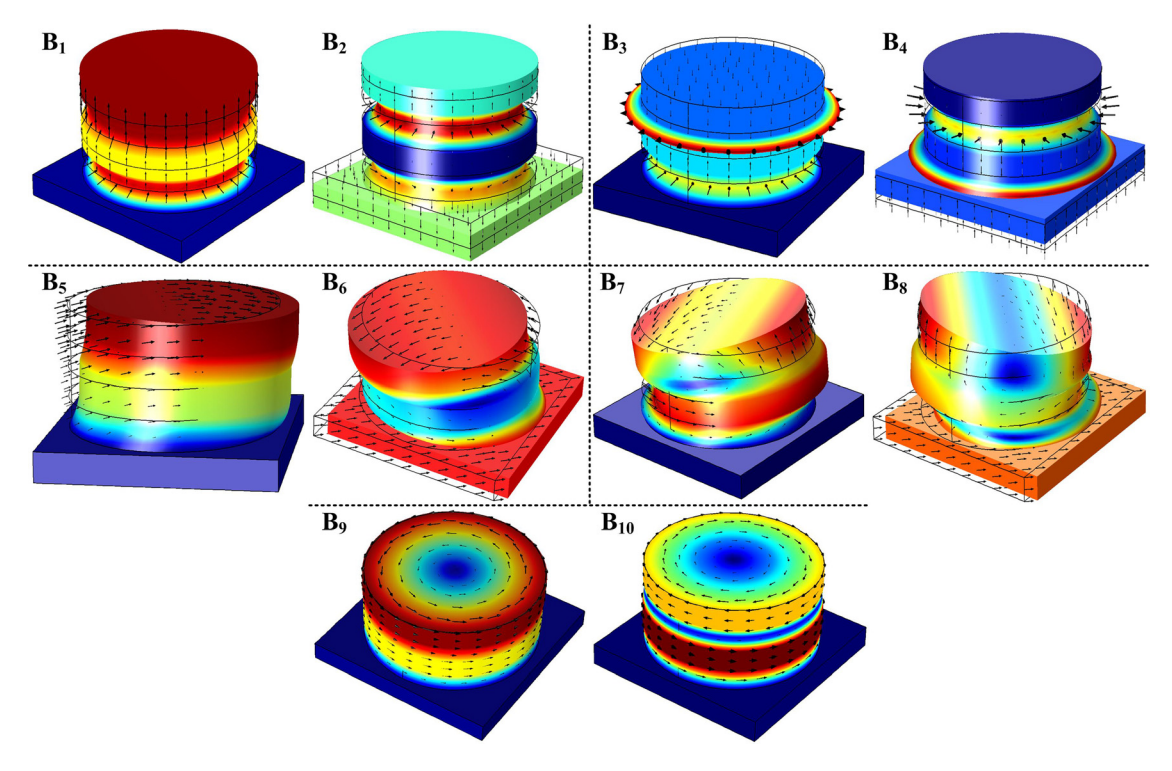


FIG. 3. The eigenmodes labeled in Fig. 2.

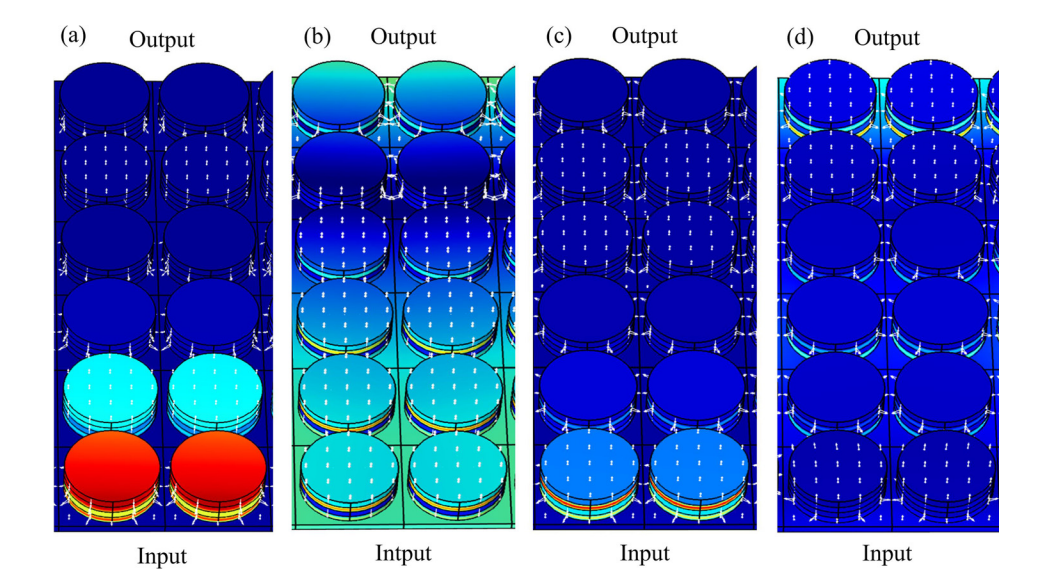
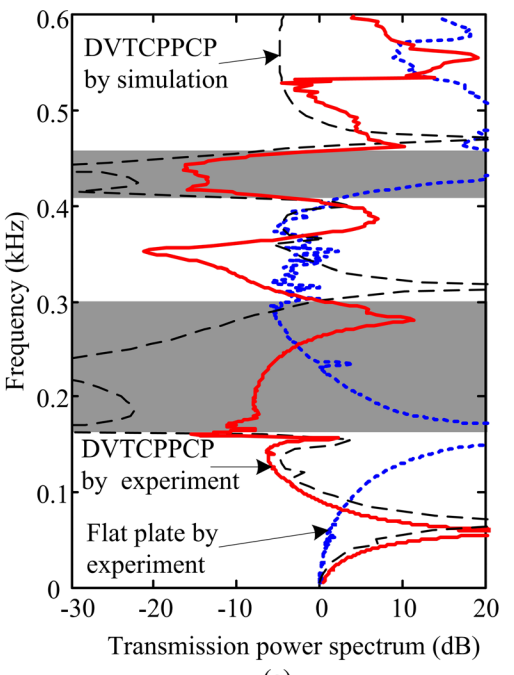


FIG. 4. Local views of the vibration modes at the starting and cutoff frequencies of first two FVBGs in the DVTCPPCP with $6a \times 6a$ unit cells: (a) 145 Hz; (b) 266 Hz; (c) 365 Hz; and (d) 411 Hz.

and B_5 , as shown in Fig. 3. Furthermore, at the starting frequencies (145 Hz and 365 Hz), the vibrations are mainly localized at the input terminal and the response at the output terminal is very small. At the cutoff frequencies (266 Hz and 411 Hz), the displacement occurs in the entire base plate along the thickness direction, which means the end of the gaps.

To further demonstrate the existence of the FVBGs of the studied structures, the flexural vibration transmission power spectrum (as shown in Fig. 5(a)) of a doubly clamped DVTCPPCP ($8a \times 2a$) is measured by flexural vibration experiments (as shown in Fig. 5(b)). A flat plate (without pillars) with same size of the DVTCPPCP ($8a \times 2a$) is placed in the control experiment. The scanning acceleration excitation is applied to the test samples from the shaking table. And the vibration transmission power spectrum is obtained by processing the signal data of the input and output accelerometers.

The grey shaded areas in Fig. 5(a) correspond to the theoretical FVBGs as shown in Fig. 2(b). One can find that the attenuation range of the measured transmission power spectrum of the doubly clamped DVTCPPCP well matches the frequency range of the theoretical FVBGs, which indicates the existence of the first two FVBGs. In contrast to the transmission power spectrum of the flat plate, the DVTCPPCP also shows obvious isolation effect of flexural vibration. However, the natural frequency of the plate is lowered by the additional weight of the pillars. The transmission power spectrum from finite element simulation in Fig. 2(a) is also compared with the experimental results. Although the attenuation range of the transmission loss from finite element simulation matches the attenuation range of the measured transmission power spectrum, some difference between them does exist. The difference could be caused by the simplifications of the finite element simulation, such as the boundary



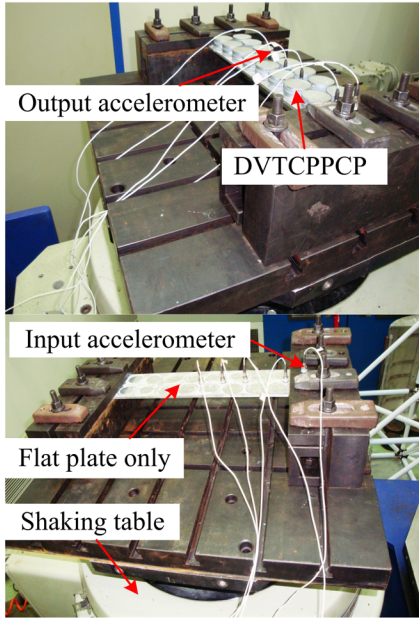


FIG. 5. (a) Comparison of the flexural vibration transmission power spectrums by finite element simulation and (b) flexural vibration experiments.

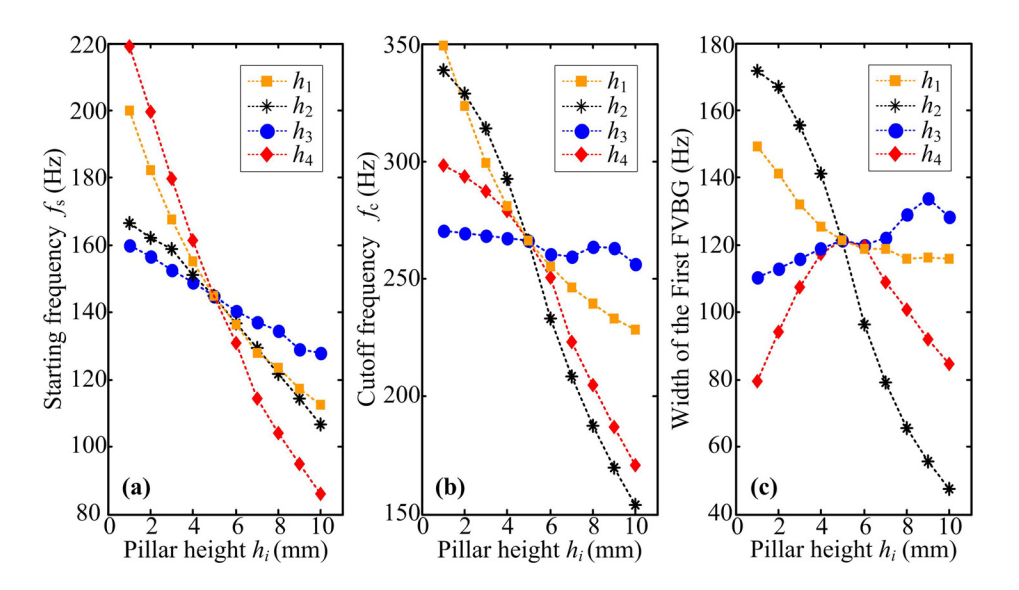


FIG. 6. First FVBG as a function of the height of each layer of the pillar: (a) f_s , (b) f_c , and (c) width of the gap.

conditions of neighbouring components, the error of material parameters, and the ignoring of the damping and viscoelasticity effect of the rubber layers. After all, the attenuation ranges of the transmission loss from finite element simulation and from the experimental results both match well the frequency range of the theoretical FVBGs.

B. Influence of geometry parameters on the FVBGs

Although a simplified spring-mass model can be built to estimate the starting and cutoff frequencies of the gaps in LR PC structures, the accurate expressions of equivalent mass and equivalent spring stiffness are difficult to determine. In addition, when the contact area increases indefinitely, the pillared PC plate with pillars composed of rubber stub and steel cap becomes a constrained layer damping plate. Thereby, the geometric size of the pillars should be taken into account and steel caps cannot be simply treated as the whole lumped mass. To analyze the influences of geometric parameters on the FVBGs, the most reliable method is using FEM to calculate the band structures.

To investigate the influences of the heights of steel caps and the rubber stubs on the FVBGs in the DVTCPPCP, the unified geometric parameters are taken as $a = 50 \,\mathrm{mm}$, e = 5 mm, and d = 45 mm. The heights of three layers of the four layers $(h_1, h_2, h_3, \text{ and } h_4 \text{ as shown in Fig. 1(b)})$ are limited to 5 mm, while the rest layer ranges from 1 mm to 10 mm. Fig. 6 shows the influences of the height of each pillared layer on the first FVBG of the DVTCPPCP. Figs. 6(a) and 6(b) indicate that f_s and f_c of this gap shift to a lower frequency when any layer of h_1 - h_4 increases. Slopes of the curves represent the sensitivity of f_s and f_c of this gap with the height change of each layer. The f_c , f_s , and the band width of the first FVBG can be adjusted in the largest range by changing h_2 , h_4 , and h_2 , respectively. The band width decreases as h_1 and h_2 increase and shows a trend of increase with the increase of h_3 . And the increase in h_4 obtains a band width, which first increases and then decreases, attaining its maximum when $h_4 = h_1 = h_2 = h_3$.

Fig. 7 shows the influences of the height of each pillared layer on the second FVBG. The slopes of curves in Figs. 7(a) and 7(b) indicate that f_s and f_c of this gap decrease with the increase in the height of each layer. Moreover, the f_c , f_s , and the band width of the second FVBG can be adjusted in the largest range by changing h_4 , h_2 , and h_4 , respectively. From Fig. 7(c), it can be found that the width of the second FVBG

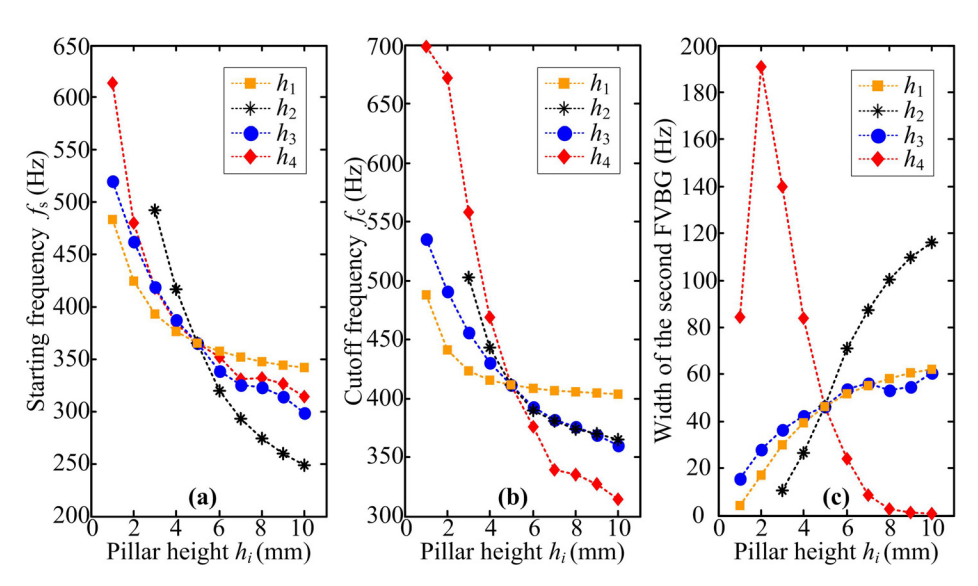


FIG. 7. Second FVBG as a function of the height of each layer of the pillar: (a) f_s , (b) f_c and (c) width of the gap.

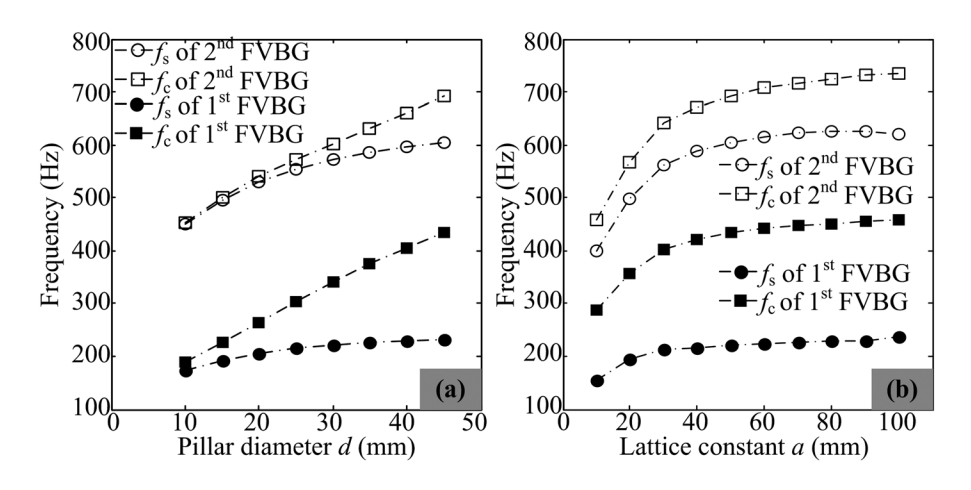


FIG. 8. Starting and cutoff frequencies of the first two FVBGs as a function of (a) the pillar diameter *d* and (b) the lattice constant *a*.

gets wider as h_1 , h_2 , and h_3 increase, but shows a tendency of decrease with the increase in h_4 . Given the above, the height of the two rubber layers (h_2 and h_4) has a greater influence on the first two FVBGs than that of the two steel caps (h_1 and h_3). However, according to the assumption of the simplified spring-mass model, it is easy to get an opposite conclusion. That is to say, that the increased height of steel layers is more helpful to increase the equivalent mass than that of the rubber layers. Thus, the simplified spring-mass model is not accurate for the pillared PC plate.

If the contact area between the pillars and the base plate is big enough, the characteristic of the pillared PC plate is obviously different from the case of a base plate with periodic spring-mass vibrators in Ref. 19. Hence, as characterization parameters of the contact area, the pillar diameter and the lattice constant need to be considered. During the calculation, we fix the thickness of the plate (e = 5 mm), the height of steel caps $(h_1 = h_3 = 5 \text{ mm})$, and the rubber stubs $(h_2 = h_4 = 2.5 \text{ mm})$. To investigate the influence of the pillar diameter d, the lattice constant is fixed as $a = 50 \,\mathrm{mm}$, and d ranges from 10 mm to 45 mm. While to investigate the influence of the lattice constant a, the pillar diameter is fixed as d = 0.9a, and a ranges from 10 mm to 100 mm. Fig. 8 shows the starting and cutoff frequencies of the first two FVBGs in the DVTCPPCP as a function of the lattice constant and the pillar diameter. As shown in Fig. 8(a), f_s and f_c of the first two FVBGs both increase with the increase in the pillar diameter d; furthermore, the increased rate of f_c is greater than that of f_s , which widens the two gaps. Fig. 8(b) indicates that f_s and f_c of the gaps increase as lattice constant a rises, and when $a > 30 \,\mathrm{mm}$, the increase rate becomes slow. Overall, the influence of the pillar diameter and lattice constant on the first FVBG is greater than that on the second FVBG.

C. Supercell of single and double vibrators

A $2a \times 2a$ supercell composed of two unit cells of the DVTCPPCP and two unit cells of the UVTCPPCP are given in Fig. 9(b). Fig. 9 shows the comparison of band structures of the UVTCPPCP (Fig. 9(a)), the DVTCPPCP (Fig. 9(c)), and the supercell (Fig. 9(b)). The parameters used in the calculation are a = 50 mm, e = 5 mm, d = 45 mm, and the height of each pillared layer h = 5 mm.

It can be found that the band structure of the supercell is not a simple superposition of the bands of the UVTCPPCP and the DVTCPPCP. In the frequency range from 0 Hz to 600 Hz, the UVTCPPCP has one FVBG (from 228 Hz to 377 Hz), the DVTCPPCP has two FVBGs (the first from 139 Hz to 266 Hz and the second from 361 Hz to 411 Hz), while the supercell has three FVBGs (the first from 140 Hz to 179 Hz, the second from 232 Hz to 320 Hz, and the third from 363 Hz to 401 Hz). One can find that all the flat bands in Figs. 9(a) and 9(c), which have nothing to do with the formation of the FVBGs, are shown in Fig. 9(b) at the same position. However, the bands involved in the formation of the FVBGs change in the supercell PC plate. Taken as a whole, the starting frequency of the first gap and the cutoff frequency of the third band gap of the supercell are approximate with the starting frequency of the first gap and the cutoff frequency of the second gap of the DVTCPPCP.

To further investigate the three FVBGs of the supercell PC plate, eigenmodes (labeled in Fig. 9(b)) corresponding to the starting and cutoff frequencies are given in Fig. 10. In mode C_1 , the vibration energy concentrates on the vertical vibration of the two steel layers in the pillars with four layers, which is similar with mode B_1 (as shown in Fig. 3). That is to say, the starting frequency of the first gap of the supercell is determined by that of the first gap of the DVTCPPCP. In mode C_2 , which corresponds to the cutoff

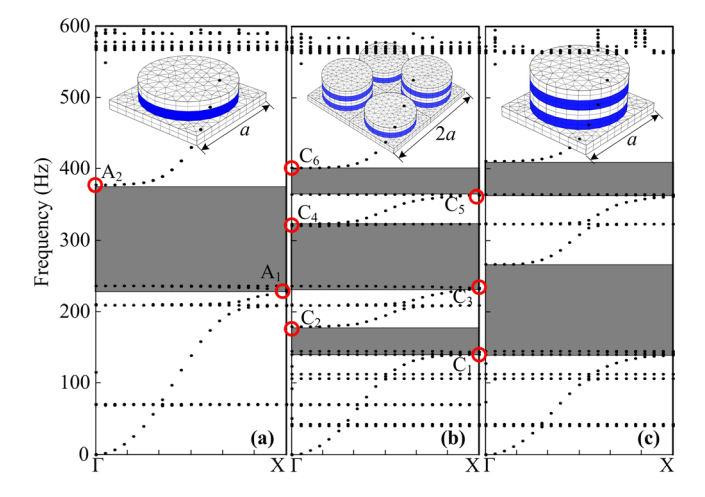


FIG. 9. Band structures of (a) the UVTCPPCP, (c) the DVTCPPCP, and (b) the $2a\times 2a$ supercell.

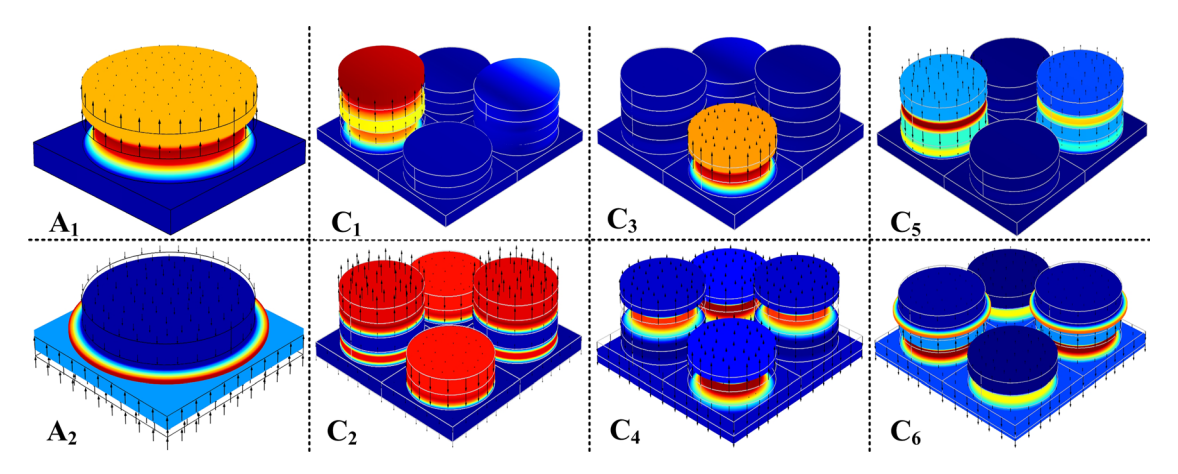


FIG. 10. Eigenmodes labeled in Fig. 9.

frequency of the first gap of the supercell, the base plate and the steel caps in the pillars with two layers do reverse vibration of the lateral steel caps of the pillars with four layers. Similarly, as the mode corresponds to the starting frequency of the second gap in the supercell PC plate, the vibration energy distribution of mode C_3 is similar with that of mode A_1 , which corresponds to the starting frequency of first gap of the UVTCPPCP. At the end of this gap (mode C_4), the inverse vibration of the four lateral steel caps of the supercell and the base plate achieves dynamic balance. Similarly, at the starting frequency of the third gap of the supercell, the vibration energy distribution of mode C_5 is similar with that of mode C_5 is similar with that of mode C_6 shows a coupling of mode C_6 and mode C_6 and mode C_6 shows a coupling of mode C_6 and mode C_6

It can be found that the starting frequencies of all the three FVBGs of the supercell match the starting frequencies of the gaps of the UVTCPPCP and DVTCPPCP, while the cutoff frequencies of the three FVBGs of the supercell are affected by the coupling of the UVTCPPCP and DVTCPPCP. Taking advantage of this supercell PC plate, the number and location of FVBGs can be designed according to the actual needs.

IV. CONCLUSIONS

In this study, we propose the DVTCPPCP and analyze its FVBGs and LVBGs by using FEM. The mechanism of the starting and cutoff frequencies of each gap is analyzed according to their corresponding eigenmodes. For the vibration attenuation in the frequency range of the FVBGs, which is much stronger than that of the LVBGs, this work takes the FVBGs of the proposed DVTCPPCP as the main object of study. Results of a flexural vibration experiment verify the existence of the FVBGs in the DVTCPPCP. The influence of the lattice constant, the height, and diameter of the pillars on the FVBGs are investigated. The height of the four layers of the double-vibrator pillars has different influence on the first two FVBGs. In general, changing the height of two rubber stubs can adjust the gaps in the largest frequency range. Both

the starting and cutoff frequencies of the first two FVBGs increase as the pillar diameter and the lattice constant rise, and the increase rate of the cutoff frequency is faster than that of the starting frequency, which broadens the band gaps. Moreover, a supercell composed of unit cells of the DVTCPPCP and the UVTCPPCP is investigated, and this supercell can be used to design plates with bandpass characteristics. The results of this study provide a new idea for the optimization of the vibration band gap in three-component pillared PC plates.

ACKNOWLEDGMENTS

The authors gratefully acknowledge the financial support from the "111 project" (Grand No. B07018).

¹M. M. Sigalas and E. N. Economou, J. Sound Vib. **158**, 377 (1992).

²M. S. Kushwaha, P. Halevi, L. Dobrzynski, and B. Djafari-Rouhani, Phys. Rev. Lett. **71**, 2022 (1993).

³Z. Liu, X. Zhang, Y. Mao, Y. Zhu, Z. Yang, C. Chan, and P. Sheng, Science 289, 1734 (2000).

⁴X. Zhou, X. Liu, and G. Hu, Theor. Appl. Mech. Lett. **2**, 041001 (2012).

⁵T. Wu, Z. Huang, T. Tsai, and T. Wu, Appl. Phys. Lett. **93**, 111902 (2008)

⁶J. Hsu, J. Phys. D: Appl. Phys. 44, 055401 (2011).

⁷P. Wang, T. Chen, K. Yu, and X. Wang, J. Appl. Phys. **113**, 053509 (2013).

⁸O. R. Bilal and M. I. Hussein, Appl. Phys. Lett. **103**, 111901 (2013).

⁹Y. Li, T. Chen, X. Wang, K. Yu, and W. Chen, J. Appl. Phys. **115**, 054907 (2014).

¹⁰Y. Pennec, B. Djafari-Rouhani, H. Larabi, J. O. Vasseur, and A. C. Hladky-Hennion, Phys. Rev. B 78, 104105 (2008).

¹¹M. Oudich, Y. Li, B. M. Assouar, and Z. Hou, New J. Phys. **12**, 083049 (2010).

¹²B. D. Rouhani, Y. Pennec, E. H. El Boudouti, J. O. Vasseur, Y. El Hassouani, C. Li, A. Akjouj, and D. Bria, Appl. Phys. A 103, 735 (2011).

¹³M. B. Assouar and M. Oudich, Appl. Phys. Lett. **100**, 123506 (2012).

¹⁴H. Zhang, J. Chen, and X. Han, J. Appl. Phys. **112**, 054503 (2012).

¹⁵K. Yu, T. Chen, and X. Wang, Physica B **416**, 12 (2013).

¹⁶Y. Xiao, J. Wen, L. Huang, and X. Wen, J. Phys. D: Appl. Phys. 47, 045307 (2014).

¹⁷M. B. Assouar, J. Sun, F. Lin, and J. C. Hsu, Ultrasonics **54**, 2159 (2014).

¹⁸A. Bergamini, T. Delpero, L. De Simoni, L. D. Lillo, M. Ruzzene, and P. Ermanni, Adv. Mater. 26, 1343 (2014).

¹⁹Y. Xiao, J. Wen, and X. Wen, J. Phys. D: Appl. Phys. 45, 195401 (2012).